Catalysis Today 146 (2009) 177–182

Contents lists available at ScienceDirect

Catalysis Today

journal homepage: www.elsevier.com/locate/cattod

Photocatalytic water splitting for hydrogen production under visible light on Ir and Co ionized titania nanotube

M. Alam Khan [1], O-Bong Yang *

School of Semiconductor and Chemical Engineering, Solar Energy Research Center, Chonbuk National University, Dukjin dong, Dukjin Gu, Jeon-ju 561-756, Republic of Korea

ARTICLE INFO

Article history:
Available online 31 March 2009

Keywords:
Water splitting
Hydrogen production
Titania nanotube
Ir and Co
Visible light

ABSTRACT

Highly dispersed iridium and cobalt metal particles (average 3 nm) were introduced in the texture of the synthesized titania nanotube (TiNT) by ion-exchange method, which were found to be effective photocatalysts for the production of stoichiometric hydrogen and oxygen by the splitting of water under the visible light irradiation. Thus prepared Ir(IE)/TiNT and Co(IE)/TiNT catalysts evolved hydrogen at the rate of 7.05 μmol/h/0.5 g and 1.27 μmol/h/0.5 g in aqueous methanol and 2.73 μmol/h/0.5 g and 0.67 μmol/h/0.5 g in pure water, respectively. The band gap energies were decreased to 2.5 eV and 2.6 eV from 3.1 eV of bare TiNT by introducing highly dispersed Ir and Co nanoparticles in the texture of TiNT, respectively, resulting in the improved photo-response towards visible light. However, visible light photo-activity for water splitting was not observed on the large aggregated Ir and Co particles on TiNT prepared by impregnation method. The prepared catalysts were characterized by FE-SEM, HR-TEM, SEMEDX, XRD, UV–vis DRS spectra, photocurrent density and BET surface area.

1. Introduction

Nanomaterials have been shown to behave quite differently from their bulk counterparts due to the effect of their quantum confinement imposed upon the charge carriers [1]. Since the photo-induced decomposition of water on TiO_2 electrodes was discovered by Fujishima and Honda [2], titania-mediated semiconductor photocatalyst has attracted extensive interest towards the process of splitting of water into hydrogen and oxygen with the use of sunlight due to their low cost method of hydrogen production [3]. One particular focus point is the development of titania-based photocatalysts capable of using visible light. However, its widespread use is impaired by the wide band gap energy (3.2 eV), which requires UV irradiation for its photocatalytic activations. Furthermore, UV light accounts for only 6% compared to 45% visible light in solar radiation. Despite of these limitations, TiO_2 still remains the most promising photo-catalyst owing to its low cost, chemical inertness, nontoxic, high efficiency and high photostability [4–7]. Especially, TiO_2 nano-particles less than 10 nm show significant photo-activity due to quantum size effects [8,9]. So, any shift in the optical response from UV to visible range spectra will have profound positive effect on the photocatalytic efficiency of the TiO_2-based photocatalysts [10]. A series of semiconductor and metal nanoparticles have been shown to facilitate charge rectification and extend the photo-response [11–15]. For that purpose, two approaches have been applied to extend the shift towards visible range: one is metal doping into TiO_2, which suffers from the thermal instability of doped metal [16]; the other is high energy ion implantation by bombarding metal ions [17,18], which is considered as an expensive method even though very effective tool. Justicia et al. demonstrated that the titania in anatase phase with large oxygen deficiency can act as an efficient photocatalyst [19]. The reduced form of titania may introduce the localized oxygen vacancy states located at 0.75–1.18 eV below the conduction band minimum of TiO_2 [20], which may improve the photo-response of the titania materials.

In our previous work, well-grown titania nanotube, and TiNT (with ca. 8 nm diameter and 500–700 nm length) possess oxygen deficiency with sodium counter cation [21], which may facilitate ion-exchange or proton exchange to introduce precious metals inside or outside of their tubular network. In the present study, we have applied reduced forms of TiO_x nanotube ($x < 2$) along with the metal doping (Ir and Co) to enhance the optical response towards visible. It was found that the photo-response in visible light was drastically improved by introducing the highly dispersed Ir and Co in the texture of TiNT by ion-exchange method, resulting in the significant activity in the water splitting reaction to produce stoichiometric hydrogen and oxygen under visible light.

* Corresponding author. Tel.: +82 63 270 2313; fax: +82 63 270 2306.
E-mail address: obyang@chonbuk.ac.kr (O.-B. Yang).
[1] Present address: School of Display and Chemical Engineering, Yeungnam University, Gyeongsan, Republic of Korea.

0920-5861/$ – see front matter © 2009 Published by Elsevier B.V.
doi:10.1016/j.cattod.2009.02.021

2. Experimental

2.1. Preparation of catalyst

The titania nanotubes (TiNTs) were synthesized from the TiO_2 nanoparticles that were prepared by sol–gel method as follows. The mixture of TiO_2/SiO_2 mole ratio of 90:10 was obtained by mixing 26 ml titanium isopropoxide (TTIP, $Ti[OCH(CH_3)_2]_4$, >99%, Junsei Chemical Co.) and 2.6 ml tetraethyl orthosilicate (TEOS, $Si(OC_2H_5)_4$ >99%, Acros Organics), and was dissolved in the 26 ml ethanol (99.5%). After refluxing the resulting solution at room temperature for 1 h, the other mixture of 26 ml ethanol and 20.3 g of 4 M aqueous HCl (36%, Showa Chemical Co.) was added slowly to the TTIP containing the former solution and further stirred at room temperature for 1 h. To form the precipitation of xerogel, thus prepared sol was put into the incubator at 80 °C for 48 h. Then, xerogel was dried and calcined in the air at 600 °C for 3 h, which were the high crystalline TiO_2 nanoparticles with an anatase phase and ca. 20 nm size.

TiO_2 nanotube (TiNT) in this study was prepared similar to Kasuga et al. [22] except the hydrothermal temperature in an aqueous NaOH (8 M) was maintained at 130 °C for 20 h in a Teflon lined autoclave vessel under continuous stirring at 200 rpm. After natural cool down to the room temperature of the autoclave, the obtained titanium dioxide white powder of nanotubular matrix was transferred into a vessel (round flask) containing distilled water and decantated in this vessel by pouring the fresh distilled water for several times. After the filtering and washing, the obtained white powder was dried and calcined in air at 80 °C and 250 °C, respectively. The obtained sample was denoted as titania nanotube.

The Ir and Co metals were introduced on TiNTs by ion-exchange or impregnation method. Chloropentaammineiridium(III) chloride ($[IrCl(NH_3)_5]Cl_2$, 99.9%, Alfa Aesar) and cobalt(II) nitrate hexahydrate ($Co(NO_3)_2{\cdot}6H_2O$, 99.9%, Aldrich) were used as a cation exchange precursors of Ir and Co metal, respectively. For the cation exchange of TiNT containing 2.7% Na^+ ion, 0.025 M aqueous solution of Ir or Co metal were introduced in the flask containing TiNT, which was stirred and maintained at the pH 10 by adding the aqueous ammonia solution at room temperature for 20 h. $IrCl(NH_3)_5^{2+}$ or Co^{2+} exchanged TiNTs were filtered, washed, dried and calcined at 250 °C in an air for 2 h, which were denoted as Ir(IE)/TiNT and Co(IE)/TiNT. The Ir and Co metal loading was 1.8 wt% according to the measurement of FE-SEMEDX.

Dihydrogen hexachloroiridate(IV) hydrate ($H_2IrCl_6{\cdot}xH_2O$, 99.9%, Alfa Aesar) and cobalt(II) nitrate hexahydrate (Co(N-

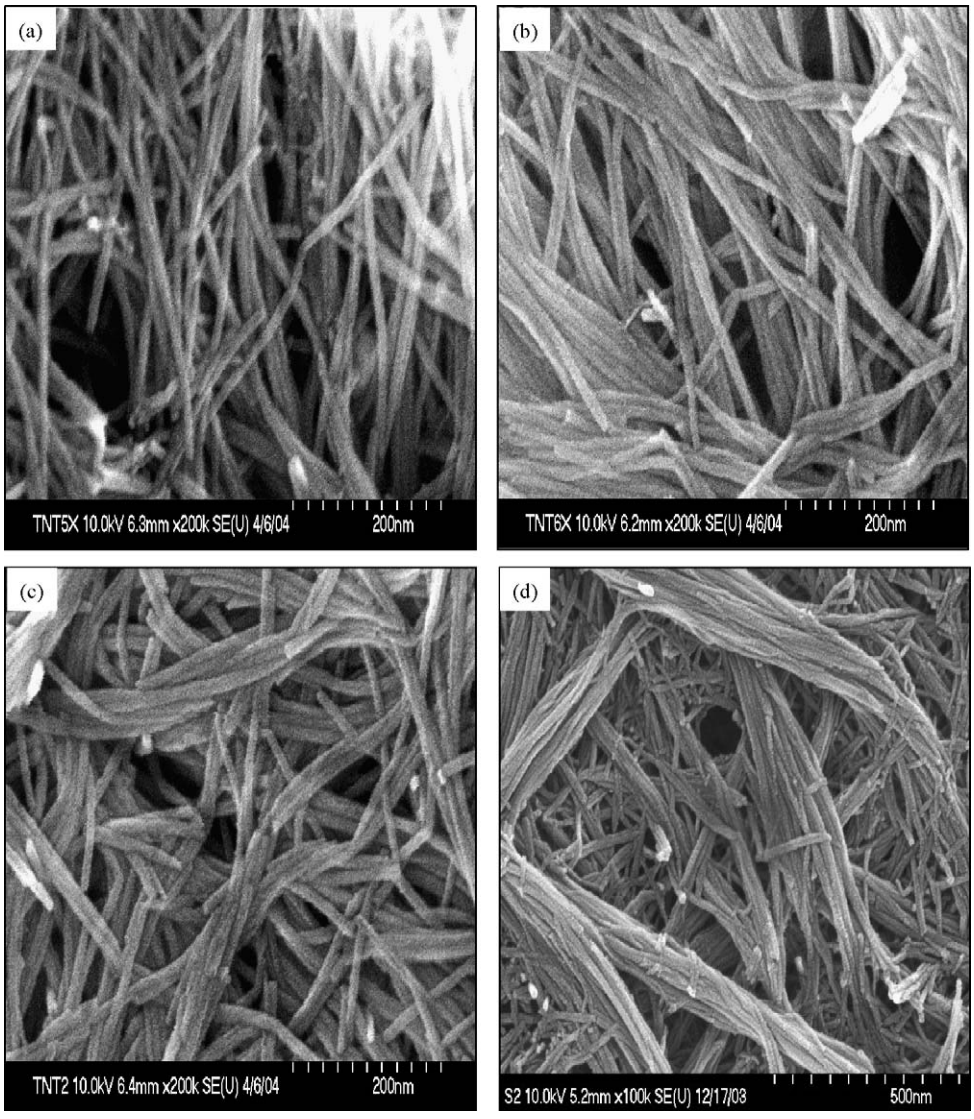

Fig. 1. FE-SEM images of (a) Ir(IE)/TiNT, (b) Co(IE)/TiNT, (c) Ir(IM)/TiNT and (d) Co(IM)/TiNT.

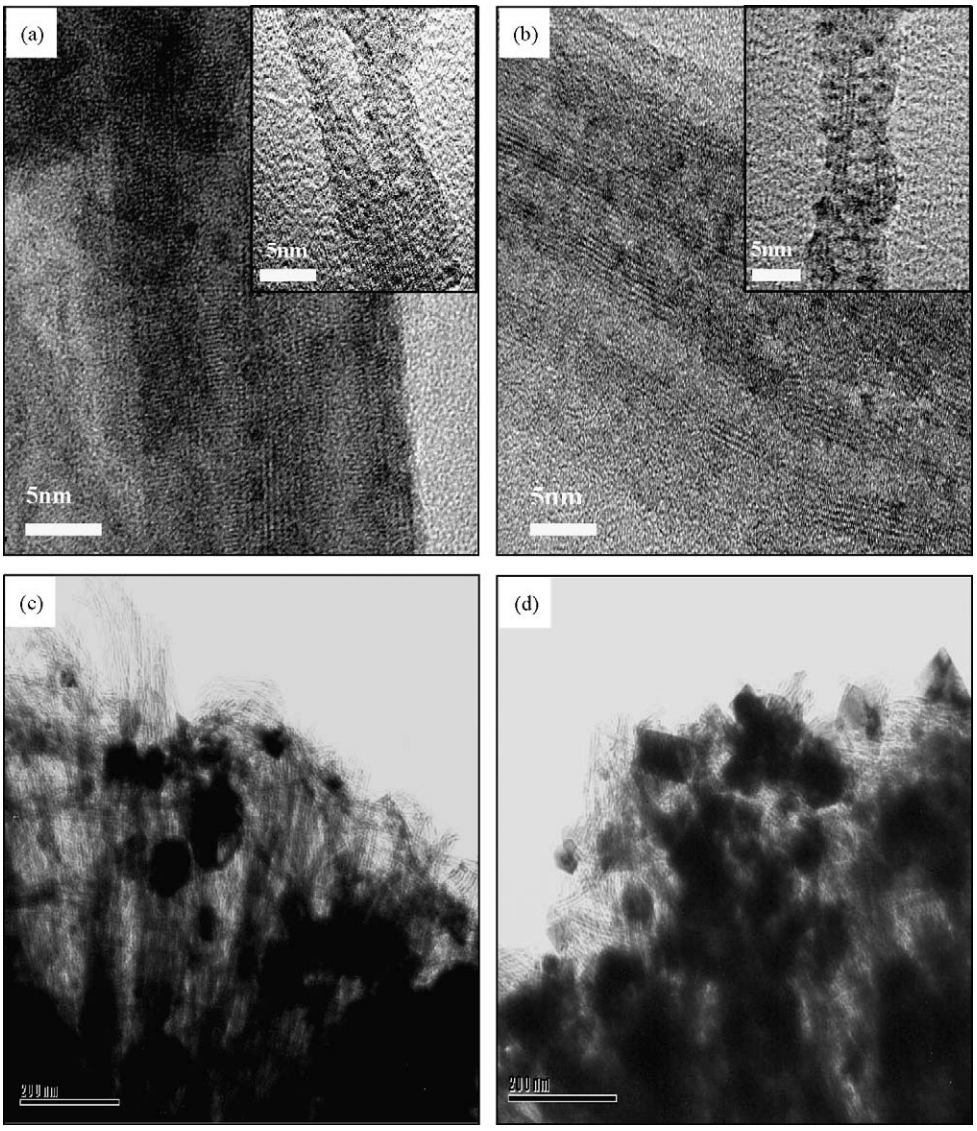

Fig. 2. HR-TEM image of (a) Ir(IE)/TiNT, (b) Co(IE)/TiNT, (c) Ir(IM)/TiNT and (d) Co(IM)/TiNT. Insets show the high magnification images.

$O_3{\cdot}6H_2O$, 99.9%, Aldrich) were used as the impregnating precursors of Ir and Co metal, respectively. For the impregnation of iridium and cobalt metals on TiNT, the slurry of TiNT and aqueous metal solutions of Ir or Co was well mixed in the rotary evaporator and dried by evaporating the water for 1 h. Ir or Co impregnated TiNT was calcined at 250 °C in an air for 2 h, which was denoted as Ir(IM)/TiNT and Co(IM)/TiNT, respectively. The Ir or Co metal loading was also maintained 1.8% in the impregnated samples for the comparison study.

2.2. Photocatalytic water splitting

The photocatalytic water splitting reaction was carried out in an outer irradiation Pyrex cell reaction system under the visible light irradiation by ozone free Xe arc lamp (300 W, Hamamatsu: L 2479) attached with UV cut filter (FSQ-GG 400 minimum spectral range of transmittance λ_1 (400) bought from Newport Corporation). In the outer Pyrex cell, 300 ml of 20% aqueous methanol or pure water slurry containing 0.5 g of a fine powder photocatalyst was well mixed by a magnetic bar during the reaction. The reaction cell was purged by bubbling with ultra-pure argon gas until dissolve oxygen is flushed out. The amounts of evolved H_2 and O_2 were quantitatively measured with 500 μl sampled gas by a gas chromatograph equipped with a thermal conductivity detector and a molecular sieve 5 Å column (30 m × 0.35 mm × 50.0 μm film thickness, HP; Ar carrier) [23,24].

2.3. Catalyst characterization

The prepared catalysts were characterized by field emission scanning electron microscopy (FE-SEM, Hitachi 4700), high resolution transmission electron microscopy (HR-TEM, Philips Technai 160 kV), scanning electron microscopy equipped with energy dispersive X-ray elemental analysis system (SEM-EDX, Hitachi 4700), X-ray diffraction (XRD, Rigaku with Cu Kα radiation), ultraviolet–visible diffuse reflectance spectra (UV–vis DRS, Shimadzu-UV 525), photocurrent density by scanning potentiostat (EG&G273) with software (EG&G M542) and BET surface area (Micromeritics ASAP 2100).

3. Results

Fig. 1 shows the FE-SEM image of the samples. The morphologies of the samples were very similar without significant breakage and deformation even after metal loading by ion-exchange and impregnation methods, indicating no adverse effect

Table 1
Physico-chemical properties of the samples.

Samples	BET surface area (m^2/g)	Band gap (eV)[a]	Metal loading (wt%)	EDX analysis (at.%)			
				M K[b]	Ti K	O K	Na K
TiNT	98	3.1	–		35	62.3	2.7
Ir(IE)/TiNT	95	2.5	1.8	1.8	34.3	63.9	0.1
Co(IE)/TiNT	92	2.6	1.8	1.9	35.0	63.0	0.1
Ir(IM)/TiNT	89	3.1	1.8	1.9	33.0	63.3	1.8
Co(IM)/TiNT	80	3.1	1.8	2.1	31.4	64.4	2.1

[a] Obtained from the data of UV–vis DRS by using the equation of 1240/λ.
[b] Atomic% of metal by FE-SEMEDX.

of ion-exchange and impregnation process on the TiNT morphology. Individual nanotubes are more separated in ion-exchanged samples as compared to impregnated samples where the intermittent bunch of nanotube bundles was observed. The nanotube bundle may be separated due to the longer magnetic stirring (20 h).

Fig. 2 shows HR-TEM images of the samples. It is notable that well dispersed Ir and Co metal particle with the average size of 3 nm are embedded on the texture of TiNTs in the ion-exchanged samples of Ir(IE)/TiNT and Co(IE)/TiNT. Partial deformation of some TiNTs was observed in the high magnification image of ion-exchanged samples as shown in the inset of Fig. 2a and b. However, large aggregated Ir and Co metal particles in the range of 10–60 nm were formed in the impregnated samples of Ir(IM)/TiNT and Co(IM)/TiNT as shown in Fig. 2c and d. The tubular structures retained as shown the fringe image of TiNT even though the formation of large aggregated Ir and Co metal particles.

The physico-chemical properties of the samples were shown in Table 1. Trace amount of sodium ions was observed in the ionized samples by the analysis of FE-SEMEDX. However, significant amount of sodium ions was remained in the impregnated samples. About 2.7% of Na^+ ion contained in TiNTs as counter cations. Most of Na^+ ions might be exchanged by metal cations of Ir and Co or NH_4^+ ions during the ion exchange. For the comparative study, same amount (1.8 wt%) of iridium and cobalt metals was introduced on TiNT by impregnation method. BET surface areas of ion-exchanged samples were slightly decreased as compared to impregnated samples, which showed the significant decreasing of BET surface area. It may be due to the coverage of bigger metal particles as observed in the TEM images of the impregnated samples.

Fig. 3 depicts the XRD patterns of the samples. Similar XRD patterns were observed in all of the samples except impregnated Co(IM)/TiNT which showed the Co metal peak at 2-theta of 35.1. The crystalline anatase peaks were observed at the 2-theta of 25.3, 38.1, 48.3, 54.3/55.1 and 62.6, which correspond to (1 0 1), (0 0 4), (2 0 0), (1 0 5)/(2 1 1), (2 0 4) phases, respectively. This is the typical titania pattern listed in JCPDS 21-1272. A small rutile peak was also observed at 2-theta of 28.1. It is consistent with the FE-SEM and HR-TEM results in terms of high dispersion of Ir and Co metal in case of ion-exchanged samples.

Fig. 4 shows the UV–vis DRS spectra of the samples. The absorption edges of the Ir(IE)/TiNT and Co/(IE)/TiNT shifted to 492 nm and 468 nm from 400 nm of TiNT, respectively. The band gap energy was estimated from absorption edge by the equation, E (eV) = 1240/λ (nm) as presented in Table 1. It is found that the well dispersed Ir and Co nanoparticles embedded in TiNT reduced the band gap energy, resulting in the visible photo-response ability in ion-exchanged samples of Ir(IE)/TiNT and Co(IE)/TiNT. However, bare TiNT and impregnated samples of Ir(IM)/TiNT and Co(IM)/TiNT do not show the visible response in UV–vis DRS spectra.

Fig. 5 shows the photocurrent densities of the samples. It was measured by using a scanning potentiostat (EG&G273), with the software (EG&G M542), as reported elsewhere [25]. The photocurrent densities were measured using the catalysts film as the working electrodes, the Pt wire as the counter electrode and an Ag/AgCl/3 M NaCl reference electrode, in an electrochemical cell (100 ml), with pH 9, 0.1 M Na_2SO_3 as the electrolyte, under visible light. As described in the literature [26] photocurrent densities are proportional to the number of photo-excited electrons. Ir(IE)/TiNT, and Co(IE)/TiNT showed high current densities in comparison with

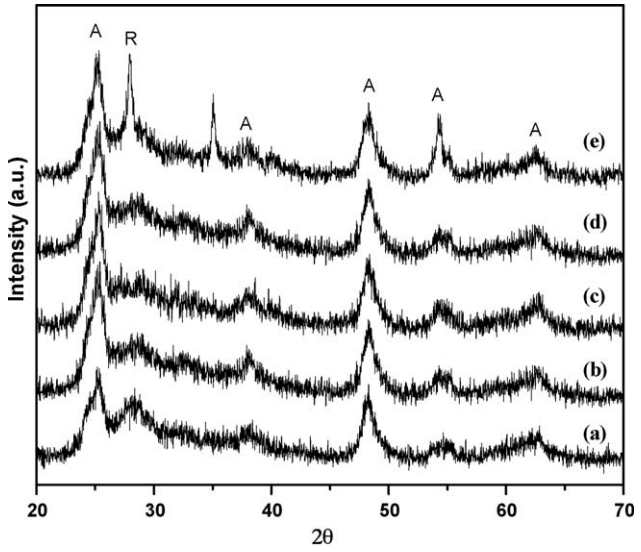

Fig. 3. XRD patterns of (a) TiNT, (b) Ir(IE)/TiNT, (c) Co(IE)/TiNT, (d) Ir (IM)/TiNT and (e) Co(IM)/TiNT. A and R means the anatase and rutile phase, respectively.

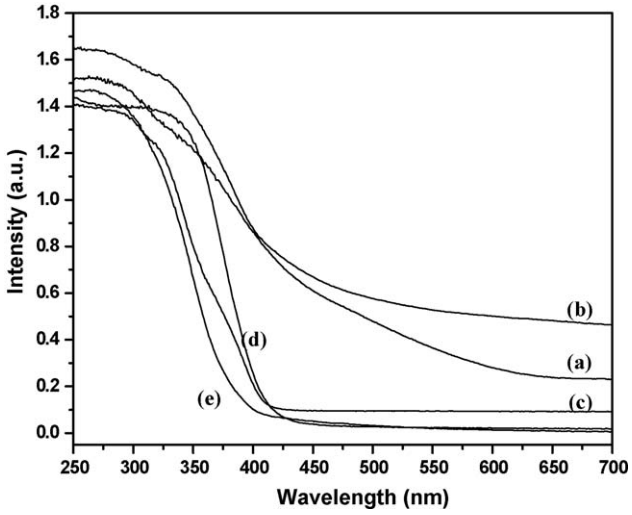

Fig. 4. UV–vis DRS of (a) Ir(IE)/TiNT, (b) Co(IE)/TiNT, (c) Ir(IM)/TiNT, (d) Co(IM)/TiNT and (e) TiNT.

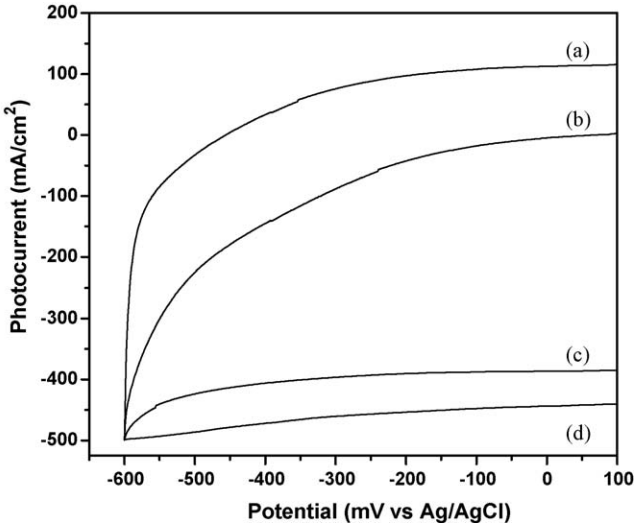

Fig. 5. Photocurrent density of (a) Ir(IE)/TiNT, (b) Co(IE)/TiNT, (c) Ir(IM)/TiNT and (d) Co(IM)/TiNT.

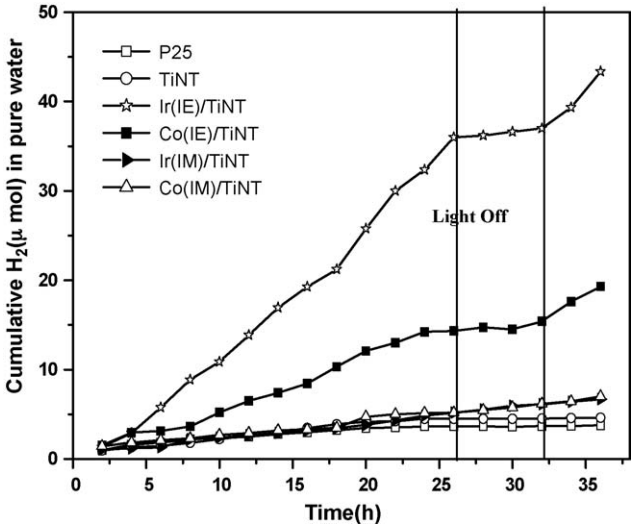

Fig. 7. Hydrogen evolution of the samples in pure water under the visible light irradiation.

the Ir(IM)/TiNT and Co(IM)/TiNT which showed very low photocurrent densities even though they contain similar amount of metals. As seen from the UV-DRS data, highly dispersed metal ionized clusters on Ir(IE)/TiNT, Co(IE)/TiNT promoted a photoresponse under visible light, resulting in high photocurrent densities. However, a significant amount of photo excited electrons may be recombined on the large aggregated Ir and Co clusters in Ir(IM)/TiNT, Co(IM)/TiNT samples, which may act as the recombination centers [30].

Figs. 6 and 7 show the cumulative evolution of H_2 in 20% aqueous methanol and pure water under visible light irradiation for 36 h, respectively. The photocatalysts of P-25 and TiNT, Ir(IM)/TiNT and Co(IM)/TiNT showed no activity for H_2 evolution in aqueous methanol and pure water under visible light. The maximum hydrogen evolution activity among the catalysts obtained on Ir(IE)/TiNT which produced the H_2 at the rate of 7.05 and 1.27 μmol/h/0.5 g in the aqueous methanol and pure water, respectively. And Co(IE)/TiNT produced 2.73 and 0.67 μmol/h/0.5 g in the aqueous methanol and pure water, respectively. Stoichiometric amount of oxygen was produced on

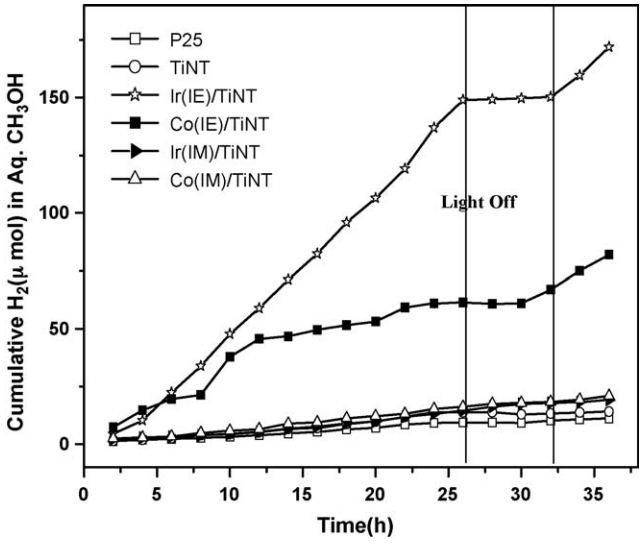

Fig. 6. Hydrogen evolution of the samples in 20% aqueous CH_3OH under the visible light irradiation.

Ir(IE)/TiNT and Co(IE)/TiNT in the aqueous methanol and pure water. The photocatalyst was not much deactivated even though reaction was carried out for 36 h. H_2 evolution was stopped in the dark (light turn off), and then the hydrogen production was resumed again by switching on the lamp without evacuation of the reactor. This indicates the H_2 production was solely based on the photocatalytic process not by tribological or mechano-catalytic process. It is well known that the enhanced photocatalytic activity in the methanol solution is attributed to the role of methanol as the hole scavenger to suppress electron and hole recombination [33,34].

4. Discussion

Haruta demonstrated that gold nanoparticles in 2–5 nm range show usually high activity [27]. Goodman and co-workers reported gold nanoparticles enhances overall energetics of titania nanoparticles [28,29]. The realization of these ultra small gold nanoparticles in titania particles lead the size effects. TiNTs have the inherent positive property of the fast electron transfer due to reduced grain boundary of 1D nanotubes nature, which may lead their better charge separations in photocatalytic water splitting reactions. The introduced nanosize metals (Ir and Co) modifies the titania nanotube surface properties by changing the distribution of electrons. The existence of the band defects states (oxygen vacancies in TiNT) just above the valence band and these vacant states overlaps with the conduction band will requires less energy for excitation of electrons from valence band. And the photo-excited electrons will be promptly transferred to metal particles owing to reduced grain boundaries of titania nanotubes, which could explain its high activities of ionized Ir(IE)/TiNT and Co(IE)/TINT. The presence of vacancies in the samples is expected to have additional effect on absorption properties of the Ir(IE)/TiNT and Co(IE)/TINT. Gerisher et al. reported that large metal of non-uniform distribution acts as recombination centers and capability of trapping photoelectron decreases [30], which may correspond to the impregnated samples of Ir(IM)/TiNT and Co(IM)/TiNT. Moreover, presence of sodium ions may also act as adverse sites to electron transfer in Ir(IM)/TiNT and Co(IM)/TiNT [31]. The band gap transitions in metal compound can be also attributed to internal transitions in metal d shell. For the same concentration of metal particles, ~3 nm particles are more effective than the larger ones as greater number of smaller particles interact and dispersed

on the photo-excited nanotubes. The Fermi level (E_f) of semiconductor is directly related to the number of accumulated electrons as illustrated by expression (1):

$$E_f = E_{CB} + kT \ln\left(\frac{n_c}{N_c}\right) \quad (1)$$

E_{CB} is the conduction band energy level versus NHE, n_c is the density of accumulated electrons, and N_c is the charge carrier density of semiconductor. As more number of metals are found on nanotube by ion-exchange method, more electrons accumulated in Ir(IE)/TiNT and Co(IE)/TINT system, which is expected a negative shift in Fermi level and by shifting the Fermi level closer to conduction band. It would be possible to improve the overall energetics of metal ion-exchanged TiNT samples. It seems that shift of Fermi level to more negative in ion-exchanged TiNT samples results in higher degree of electron accumulation. Chen et al. has reported the 0.1 eV shifting of E_F on ~2 nm Au particles [32]. Highly dispersed Ir and Co particles in the TiNT matrix may lead to fast electron transfer and reduce recombination of exciton along with shift of intrinsic absorption edge of Ir(IE)/TiNT and Co(IE)/TiNT in the visible range as depicted by the UV-DRS results in Fig. 4. The conduction band of Ir and Co ionized TiNT mainly consisted of Ti 3d and sharp Ir 5d and Co 3d orbital, while the valence band consisted of O 2p [33]. The band gap energy between the valence and conduction bands of TiNT is 3.1 eV, while the Ir 5d and Co 3d are located at 2.5 eV and 2.6 eV, respectively. When the light with wavelengths longer than 400 nm is used for irradiation, the electrons in the Ir 5d and Co 3d band are excited to the conduction band, resulting in the improved photocatalytic activity for the water splitting to produce stoichiometric amount of hydrogen and oxygen. It is still not clear how metal and transition metal ionization could enhance shift in the visible range, but it seems that nanosize effect, oxygen vacancies, reduced grain boundaries and d orbital play key roles in the extension towards visible and efficient photocatalytic activity.

5. Conclusions

Ion-exchange method was effective to introduce highly dispersed Ir and Co metal cluster around ~3 nm in the texture of the titania nanotube. Nano sized Ir and Co embedded TiNT by ion-exchange method showed the improved photo-response under visible light by reducing the band gap and shifting absorption spectra towards red region. However, the large aggregated Ir and Co particles were formed on TiNT by impregnation method, which showed negligible visible light photo-response. The maximum hydrogen evolution activity among the catalysts obtained on Ir(IE)/TiNT which produced the H_2 at the rate of 7.05 μmol/h/0.5 g and 1.27 μmol/h/0.5 g in the aqueous methanol and pure water, respectively. However, P-25 and TiNT, Ir(IM)/TiNT and Co(IM)/TiNT showed no activity for H_2 evolution in aqueous methanol and pure water under visible light. The introduced nanosize Ir and Co metal particles and oxygen deficiencies in TiNT might modify the band structure for the effective separation of exiton, resulting in improved photocatalytic water splitting activity under visible light.

Acknowledgements

We gratefully acknowledge the support from Brain Korea 21 (BK21) program and the Center for Ultra Micro Chemical Process Systems (CUPS) sponsored by KOSEF.

References

[1] C.B. Murray, D.J. Norris, M.G. Bawendi, J. Am. Chem. Soc. 115 (1993) 8706.
[2] A. Fujishima, K. Honda, Nature 238 (1972) 37.
[3] J.O'.M. Bockris, B. Dandapani, J.C. Was, in: K.W. Boer (Ed.), Advances in Solar Energy, Plenum Press, New York, 1989, p. 171 (37).
[4] N. Serpone, E. Pelizzetti, Photocatalysis and Applications, Wiley, New York, 1989.
[5] V. Kozhukharov, P. Vitanov, E. Kabasanova, K. Kabasanov, M. Machkova, V. Blaskov, D. Simeonov, G. Tzaneva, J. Environ. Prot. Eco. 2 (2001) 107–111.
[6] M. Schiavello, H. Dordrecht, Photochemistry, Photocatalysis, Photoreactors (Eds.), Photochemistry, Photocatalysis, and Photoreactors, Kluwer Academic, Boston, MA, 1985.
[7] A.L. Linsebigler, G. Lu, J.T. Yates, Chem. Rev. 95 (1995) 735.
[8] M. Anpo, T. Shima, Y. Kubokawa, Chem. Lett. (1985) 1799.
[9] (a) M. Anpo, Y. Kubokawa, Rev. Chem. Intermed. 8 (1987) 105;
(b) M. Anpo, T. Kawamura, S. Kodama, K. Maurya, T. Onishi, J. Phys. Chem. 92 (1998) 438.
[10] R. Asahi, T. Morikawa, T. Ohwaki, K. Aoki, Y. Taga, Science 293 (1998) 269.
[11] H. Gerischer, M. Luebke, J. Electroanal. Chem. 204 (1986) 225.
[12] L. Spanhel, H. Weller, A. Henglein, J. Am. Chem. Soc. 109 (1987) 6632.
[13] S. Hotchandani, P.V. Kamat, J. Phys. Chem. 96 (1992) 6834.
[14] R. Vogel, P. Hoyer, H. Weller, J. Phys. Chem. 98 (1994) 3183.
[15] C. Nasr, S. Hotchandani, W.Y. Kim, R.H. Schmehl, P.V. Kamat, J. Phys. Chem. B 101 (1997) 7480.
[16] W. Choi, et al. J. Phys. Chem. 98 (1994) 13669.
[17] (a) M. Anpo, H. Yamashita, Y. Ichihashi, Optronics 186 (1997) 161;
(b) M. Anpo, H. Yamashita, S. Kanai, K. Sato, T. Fujimoto, US Patent 6077,492 (2000).
(c) M. Anpo, Pure Appl. Chem. IUPAC 72 (2000) 1265.
[18] (a) M. Anpo, M. Takeuchi, Int. J. Photoenergy 3 (2001) 1;
(b) H. Yamashita, M. Harada, J. Misaka, M. Takeuchi, Y. Ichihashi, F. Goto, M. Ishada, T. Sasaki, M. Anpo, J. Synchrotron Radiat. 8 (2001) 561.
[19] I. Justicia, P. Ordejon, G. Canto, J.L. Mozos, J. Fraxedas, G.A. Battiston, R. Gerbasi, A. Figueras, Adv. Mater. 14 (2002) 1399.
[20] D.C. Cronemeyer, Phys. Rev. 113 (1959) 1222.
[21] M.A. Khan, H.-T. Jung, O-B. Yang, J. Phys. Chem. B 110 (2006) 6626.
[22] T. Kasuga, M. Hiramatsu, A. Hoson, T. Sekino, K. Niihara, Langmuir 14 (1998) 3160.
[23] T.-V. Nguyen, O-B. Yang, Catal. Today 87 (2003) 69.
[24] T.-V. Nguyen, K.-J. Kim, O-B. Yang, Photochem. Photobiol. 173 (2005), 56, 3160.
[25] S.R. Rao, H.R. Sahu, Indian Acad. Sci. 113 (2001) 651.
[26] T.-V. Nguyen, H.-C. Lee, O-B. Yang, Sol. Energy Mater. Sol. Cells 90 (2006) 967.
[27] M. Haruta, Catal. Today 36 (1997) 153.
[28] M. Valden, X. Lai, D.W. Goodman, Science 281 (1998) 1647.
[29] Z.X. Yang, R.Q. Wu, D.W. Goodman, Phys. Rev. B 6 (2000) 14066.
[30] H. Gerisher, Conditions for an efficient photocatalytic activity of TiO_2 particles, in: D.F. Ollis, H. Al-Ekabi (Eds.), Photocatalytic Purification and Treatment of Water and Air, Elsevier Science Publishers B.V., New York, 1993, p. 1.
[31] A. Fernandez, G. Lassaletta, V.M. Jimenez, A. Justo, A.R. Gonzalez-Elipe, J.-M. Herrmann, H. Tahiri, Y. Ait-Ichou, Appl. Catal. B 7 (1995) 49.
[32] S. Chen, R.S. Ingram, M.J. Hostetler, J.J. Pietron, R.W. Murray, T.G. Shaaff, J.T. Khoury, M.M. Alvarez, R.L. Whetten, Science 280 (1998) 2098.
[33] D.W. Hwang, W. Li, S.H. Oh, J.S. Lee, J. Phys. Chem. B 107 (2003) 4963.
[34] H. Kato, A. Kudo, J. Phys. Chem. B 105 (2001) 4285.